The Evolution and Structure of a "Bow-Echo–Microburst" Event. Part II: The Bow Echo

WEN-CHAU LEE

National Center for Atmospheric Research, Boulder, Colorado*

ROGER M. WAKIMOTO

Department of Atmospheric Sciences, University of California, Los Angeles, Los Angeles, California

RICHARD E. CARBONE

National Center for Atmospheric Research, Boulder, Colorado

(Manuscript received 29 January 1991, in final form 23 January 1992)

ABSTRACT

A bow echo is a bow-shaped radar reflectivity pattern that is often accompanied by downbursts at the apex of the bulge. It appears that there are two types of bow echoes documented in the literature, the squall-line type (SLBE) and the single-cell type (CBE). It is not clear that these two types of bow echoes are dynamically similar. This study presents the first complete case study on the CBE, which occurred on 14 July 1982 during the Joint Airport Weather Studies (JAWS) Project. The stormwide kinematic and thermodynamic structure of this storm was documented in Part I of this paper. This paper examines the initiation and evolution of a vorticity couplet using a vorticity-budget analysis to study the bow-echo structure and the bow-echo–microburst relationship.

The elongated-shaped echo assumed a bowed shape below cloud base after the downdraft developed. The bow echo is associated with a cyclonic–anticyclonic vorticity couplet with maximum relative vorticity intensities of 5×10^{-3} and -4×10^{-3} s^{-1}, respectively, at the 2.4-km height. This couplet does not exist prior to the initiation of the downdraft. Examination of the vorticity budget shows that the vertical vorticity couplet is generated primarily through tilting of ambient horizontal vorticity by the microburst downdraft. The positive vorticity is enhanced by both the stretching effect and the downward advection of positive vorticity from above that is produced by the updraft through the same mechanism. A particle-trajectory analysis shows that the elongated echo is distorted into a bow shape by the shear vorticity, which exhibits a velocity differential between the center and edges of the echo.

A conceptual evolution model of the CBE is constructed based on the vorticity analysis in which an elongated echo may deform into a bow shape under the following meteorological condition: 1) a nearly unidirectional vertical shear, and 2) downdraft development. The product of the vertical shear and the horizontal gradient of the downdraft determine the strength of the vorticity couplet and hence the extent of the echo deformation. Since the environmental shear is often weak with an airmass thunderstorm, a strong downdraft is required to form a strong vorticity couplet. This may be why a CBE is often associated with strong wind events.

1. Introduction

On 14 July 1982, an intense thunderstorm produced a strong microburst within the network of the Joint Airport Weather Studies (JAWS) Project (McCarthy et al. 1982). This case was unique for two reasons:

1) It was one of the first datasets of a microburst-producing storm that extended above the subcloud layer.

2) The radar signature of the parent storm evolved into a bow-shaped echo, a phenomenon that has attracted much attention in recent years.

Part I (Lee et al. 1992; hereafter referred to as Part I) of this study examined the kinematic and thermodynamic structure of the microburst based on multi-Doppler radar analysis and thermodynamic retrieval techniques. Emphasis was placed on the origin of the downdraft and the forcing mechanisms that intensified the downdraft to microburst intensity. In this paper, the evolution of the bow-shaped radar reflectivity signature is studied. The analyses herein will attempt to answer why the echo of the parent storm assumes this particular radar reflectivity pattern.

* The National Center for Atmospheric Research is sponsored by the National Science Foundation.

Corresponding author address: Dr. Wen-Chau Lee, NCAR, P.O. Box 3000, Boulder, CO 80307-3000.

2. Past studies of two types of bow echoes

Radar reflectivity signatures have been widely used in severe-storm nowcasts. A well-known example is the *hook echo* (Stout and Huff 1953), used as a precursor for tornado detection. Fujita (1978) discovered another radar signature, the *bow echo,* that was often associated with downbursts. This was subsequently confirmed by other studies using National Weather Service (NWS) conventional radars and aerial damage surveys (e.g., Fujita 1981; Forbes and Wakimoto 1983). As originally defined by Fujita (1978), a bow echo is an outward bulge within a line of radar echoes and in some respects is similar to the line echo wave pattern (LEWP) described by Nolen (1959). Although never explicitly discussed in previous literature, it is clear that two distinct scales of bow echoes exist—the squall-line–type bow echo (SLBE) and the single-cell–type bow echo (CBE).

SLBEs usually involve one or more bulges and concavities within a squall line. Straight-line surface-damaging winds near the apex of the bulge of the bow echo have been documented in the literature (e.g., Nolen 1959; Hamilton 1970; Fujita 1978; Forbes and Wakimoto 1983; Przybylinski and Gery 1983; Wakimoto 1983; Wright 1985). The spatial scale appears to range from a few tens to a few hundred kilometers and the temporal scale ranges from a few hours to several days. In fact, large SLBEs appear to be a type of the derecho (Hinrichs 1888) that had been documented by several investigators (e.g., Johns and Hirt 1983; Przybylinski and DeCaire 1985).

The first detailed study of an SLBE was presented in Fujita (1981). In his Fig. 23, the bulge of the bow echo was associated with a strong ground-relative rear-to-front jet (rear-inflow jet). Fujita (1981) proposed a model of this type of bow echo based on many case studies using conventional radars and one dual-Doppler radar analysis on a single scan plane. Knupp and Jorgensen (1985), Smull and Houze (1985), and Schmidt and Cotton (1989) have examined other SLBEs and concluded that the bulge or concavity was directly related to the rear-inflow jet. This jet appears to form a bow echo through two mechanisms: 1) by advecting a part of the squall line forward, and 2) by entraining dry air into the rear flank, which then erodes the back side of the echo through evaporation of hydrometeors. Recently, Weisman (1990) successfully simulated an SLBE using a three-dimensional model. He identified favorable environmental conditions, such as unidirectional vertical shear over the lowest 2.5 km (at least 25 m s^{-1}) and a convective available potential energy (at least 2000 m^2 s^{-2}). A rear-inflow jet is the result of baroclinically generated horizontal vorticity.

In contrast to the SLBE, other studies in the literature have documented a type of bow echo that evolves from a single-cell thunderstorm (Fujita and Byers 1977; Fujita and Caracena 1977; Fujita 1985; Elmore 1986). Fujita and Byers (1977) and Fujita and Caracena (1977) coined the term *spearhead echo* to describe this radar signature which, except for the smaller horizontal length scale, exhibits echo concavity similar to the SLBEs. Elmore (1986) studied a CBE that was only 10–15 km in length with low reflectivity (30 dBZ_e). Multi-Doppler analyses revealed a rear inflow associated with a weak-echo region similar to those documented in the SLBE cases. Unfortunately, owing to the coarse spatial resolution, Elmore was unable to resolve the vertical velocity.

While there have been several studies on the kinematic and dynamic structure of the SLBE, there has not been a detailed study of CBEs. The focus of this paper is on the CBE event on 14 July using the multi-Doppler radar fields presented in Part I. Particular emphasis will be placed on the echo evolution, forcing of the rear-inflow jet, and the stormwide vorticity pattern through a vorticity budget analysis. Particle trajectories are also computed to illustrate the distortion of the echo shape. A conceptual model for the CBE and the bow-echo–microburst relationship is constructed based on the vorticity budget analysis.

3. The 14 July 1982 bow echo

a. The echo evolution

Figure 1 illustrates the three-dimensional perspective of the echo evolution outlined by the 35-dBZ_e isopleth. The "eye" position is located at the storm's southwest quadrant and views into the back of the bow echo (the weak-echo region).

A well-defined surface bow echo and its associated weak-echo region are best illustrated at 1546. An elongated echo can be found at approximately 8 km at 1528 mountain standard time (MST; hereafter, all times are MST unless specified otherwise) that is conformed to the shape of the updraft. This echo descends as time progresses and evolves into a bow shape below the cloud base. After the downdraft is initiated by precipitation loading below the cloud base about 1533, the uniform easterly flow is split after the vorticity couplet formed. Both of these lag behind the leading edge of the downdraft. Schematics of the locations of the primary updrafts and downdrafts, the airflow, and the vorticity couplet at 1.6 km are also illustrated in Fig. 1. It is evident that the formation of a bow echo involves four-dimensional processes (in space and time) and basically is a subcloud phenomenon in this case.

Figure 2 illustrates the surface-echo evolution and the corresponding CP-3 Doppler radial-velocity pattern from 1536 to 1552. A reflectivity notch between the main echo and the appendage that is produced by a separate updraft (maximum reflectivity of 42 dBZ_e) is not considered a bow echo. The surface divergence was first detected by CP-3 at 1541, which is the same time that the distortion of the 40-dBZ_e echo (hatched region)

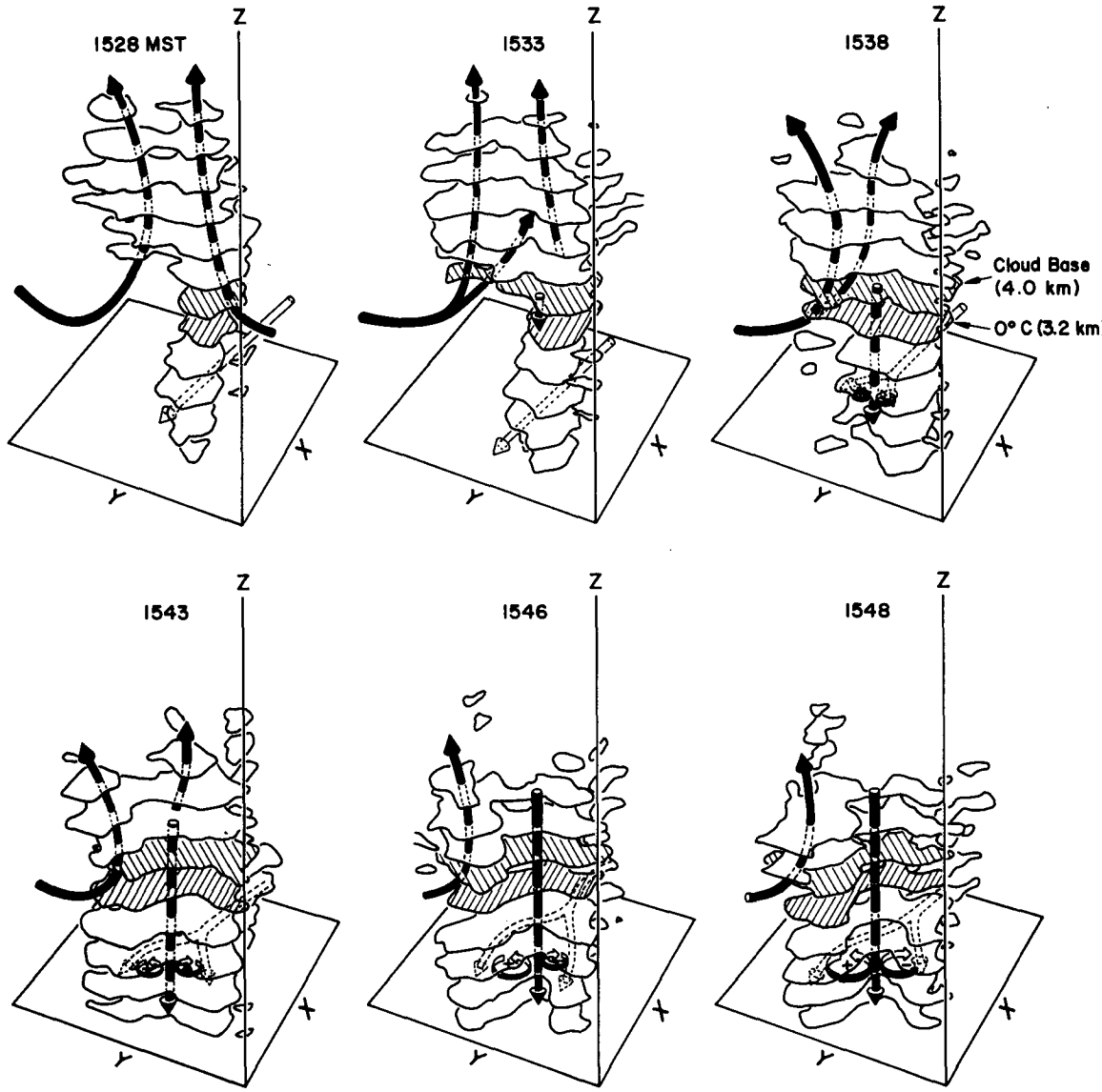

FIG. 1. The 3D perspective plots of the 14 July 1982 storm at 1528, 1533, 1538, 1543, 1546, and 1548 MST. Echoes are outlined by the 35-dBZ_e reflectivity isopleth. Also highlighted in the figure are major updraft and downdraft, the vorticity couplet, and the airflow at 1.6 km. The two hatched levels are near the cloud base (4 km) and 0°C (3.2 km).

is observed. Therefore, a surface bow echo is not a precursor of a microburst event, at least not in this case study.

The horizontal structure of a bow echo and its accompanying circulation (in ground-relative coordinates) at 1548 are illustrated in Fig. 3 [2.4 km above ground level (AGL); hereafter all heights are AGL]. A rear-inflow jet of 10 m s^{-1} is associated with the weak-echo region that has been observed commonly in previous CBE (Elmore 1986) and SLBE studies (Fujita 1981; Knupp and Jorgensen 1985; Smull and Houze 1985; Schmidt and Cotton 1989). In these past studies, it was assumed that the center part of the elongated echo was being advected forward by this rear-inflow jet. In addition, this rear-inflow jet can also entrain drier environmental air to erode the back side of the echo.

Figures 4, 5, and 6 portray the horizontal structure and evolution of this bow-echo event. By comparing the ground-relative velocity with the storm-relative velocity at 2.4 km and 1548 between Figs. 3 and 6, note that the rear-inflow jet does not exist in the storm-relative flow field. The low-level storm-relative winds (hereafter, all winds are storm-relative unless specified otherwise) below 3.2 km at 1528 (not shown) were easterly with near-zero vertical relative vorticity (here-

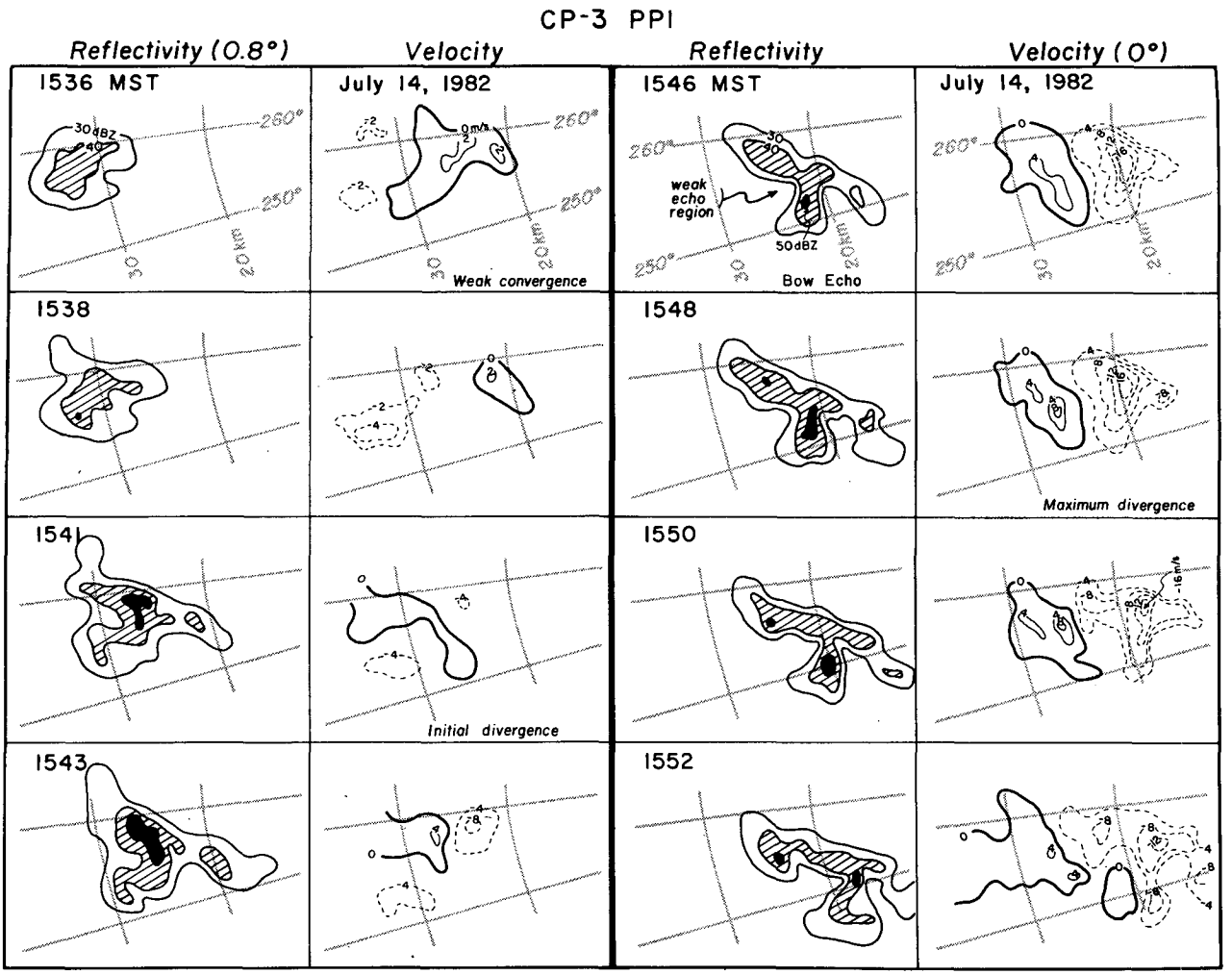

FIG. 2. Time series of CP-3 reflectivity and Doppler velocity from 1536 to 1552. The radar reflectivity data is taken from the 0.8° PPI scan to avoid ground-clutter contamination.

after, all vorticities are relative vorticities). This is also observed at 1.6 and 2.4 km and 1533 and at 1.6 km and 1538. A weak vorticity couplet exists at 3.2 km and 1533 accompanied by a slightly split easterly flow. The descending sequence of the vorticity couplet as well as the split of the easterly flow is consistent with the leading edge of the downdraft. The vorticity couplet intensifies as the downdraft strengthens after 1538 and is evident from 1.6 km up to 3.2 km after 1541. The maximum intensity of the vorticity couplet, 5×10^{-3} s^{-1} (-4×10^{-3} s^{-1}) on the north (south) side of the downdraft, occurred at 2.4 km and 1548, approximately 2 min after the passage of the maximum downdraft at this height. By examining the storm-relative vorticity in Figs. 4–6, these vorticity couplets are associated with shear in the horizontal velocity rather than a pure rotation. It is evident that the concavity of the echo first forms (as defined by the 35-dBZ_e contour) at 3.2 km and 1538 and appears at lower levels as time progresses.

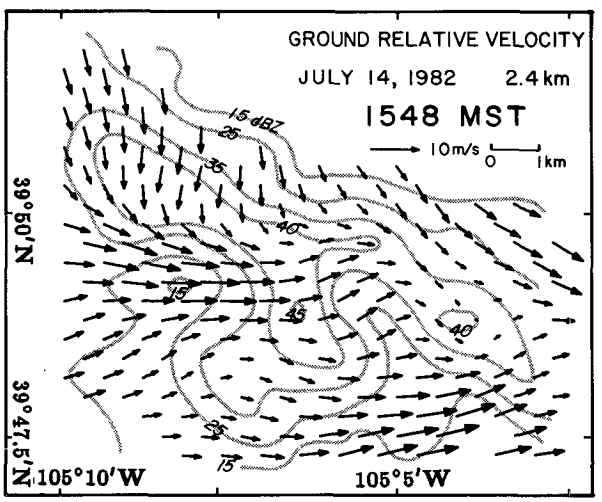

FIG. 3. Horizontal bow-echo structure at 2.4 km and 1548 MST. Vectors are the ground-relative velocities.

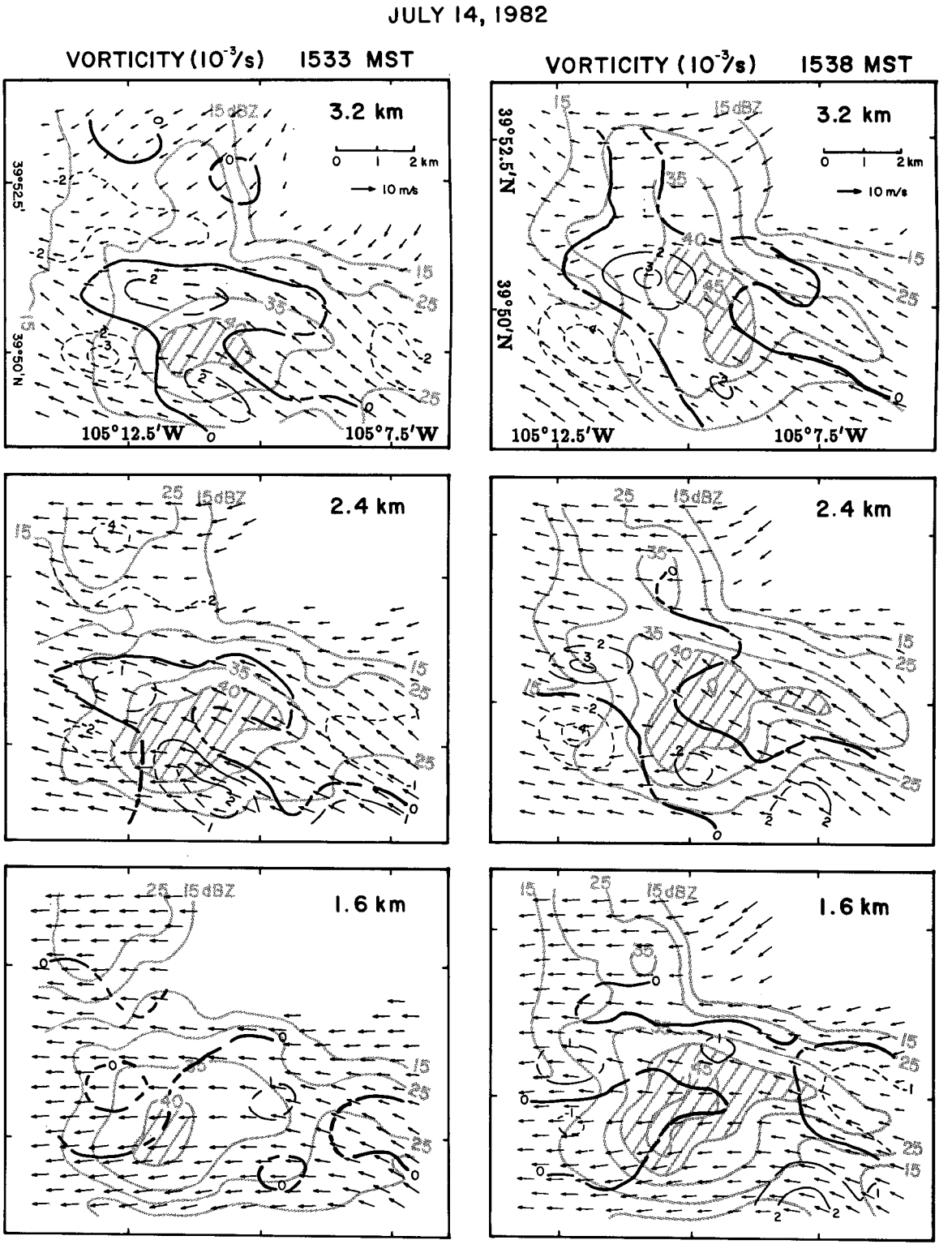

FIG. 4. Evolution of bow echo and vorticity from 1.6 to 3.2 km at 1533 and 1538 MST. Solid (dashed) lines are positive (negative) vertical vorticity (10^{-3} s^{-1}), respectively. Vectors are storm-relative velocities. Reflectivity factor (gray lines) greater than 40 dBZ_e is hatched.

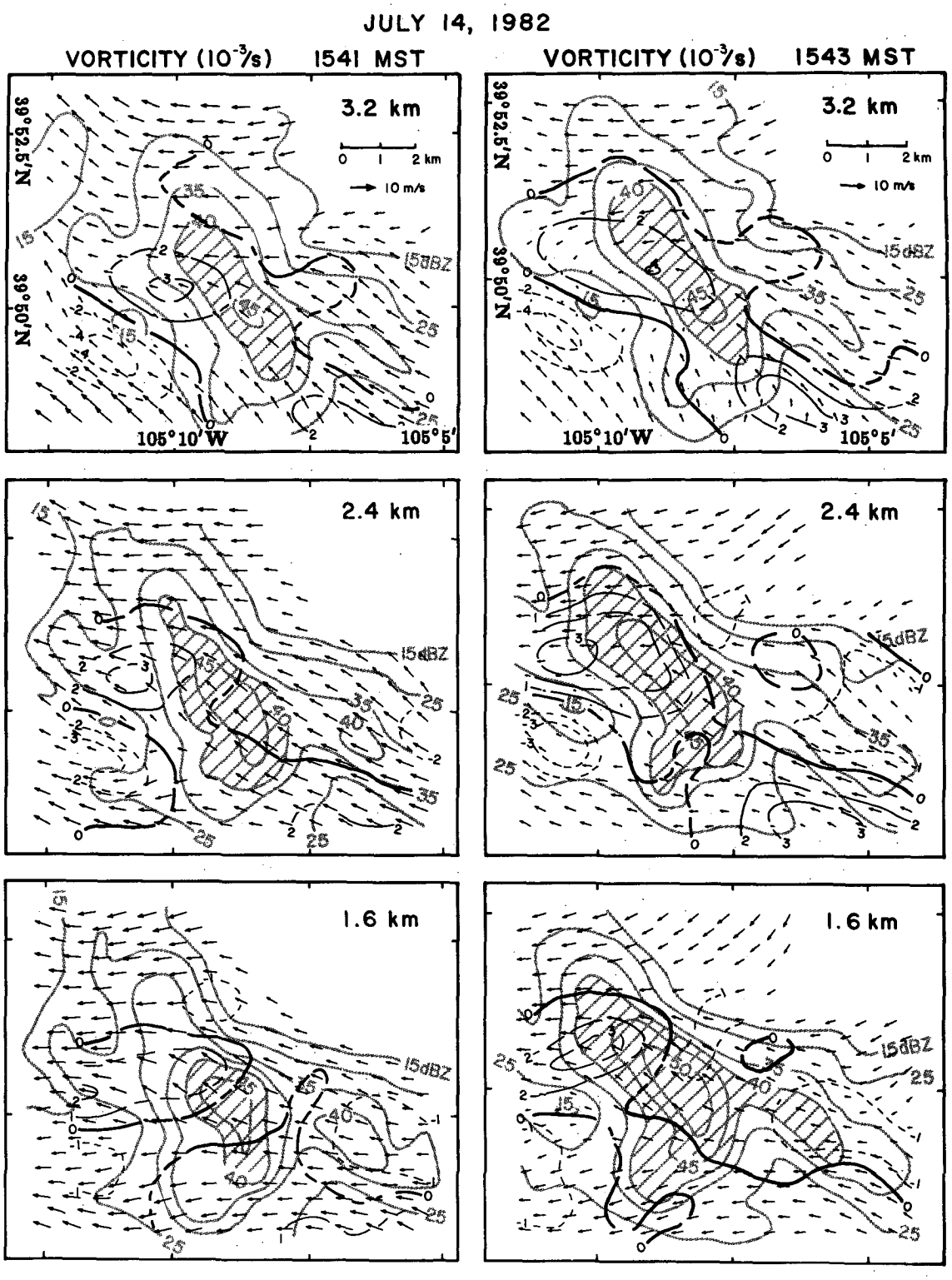

FIG. 5. Same as Fig. 4 except for 1541 and 1543 MST.

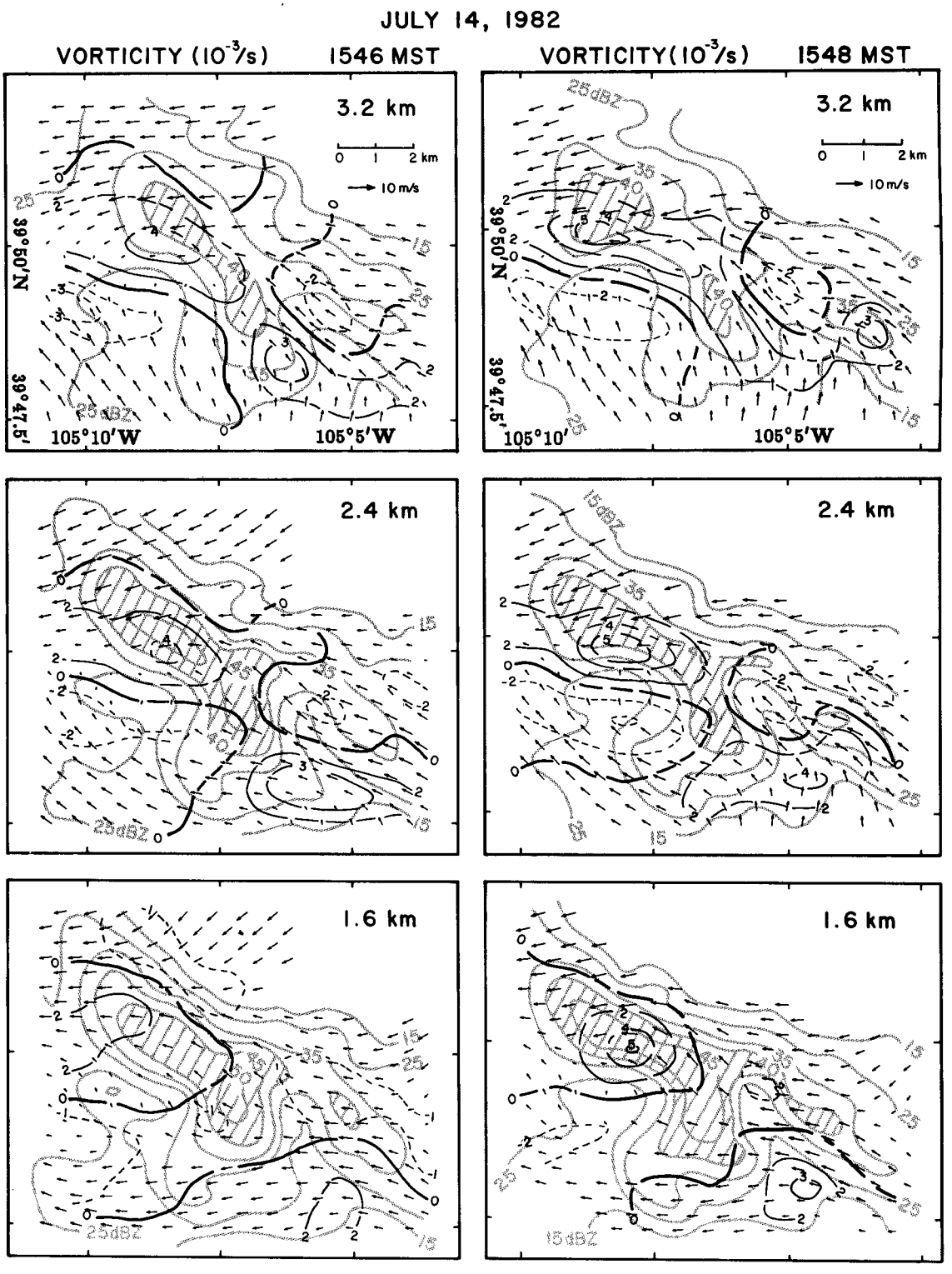

FIG. 6. Same as Fig. 4 except for 1546 and 1548 MST.

It is important to note that the distortion of the echo occurred after the formation of the vorticity couplet. The first indication of the split on the easterly flow field occurs at 3.2 km and 1533 on initiation of the downdraft. This flow pattern, together with the vorticity couplet, propagates downward as the downdraft descends and intensifies. The vorticity couplet below 0.8 km is destroyed and masked by the divergent component of the microburst outflow.

In the next subsection, we perform a particle-trajectory analysis to demonstrate the relative motion of hydrometeors within the storm caused by the vorticity-couplet circulation.

b. *Particle-trajectory analysis*

A particle-trajectory analysis is performed to trace the origin of the precipitation particles that composed the low-level bow echo. The methodology is similar to that of the air-parcel trajectories described in Miller et al. (1988). This is a complex problem since the reflectivity factor is proportional to the sixth moment of the hydrometeor size distribution within a pulse volume while the terminal velocity is also size dependent. For example, a 45-dBZ_e echo is composed of a spectrum of particles that can have different origins due to the differences in terminal fall speeds. We performed particle-trajectory analyses on several particle sizes ranging from 1 to 4 mm. To simplify the problem, we took into account only a constant terminal velocity to each size category without correcting density variation with height and without computing particle growth. Only the trajectories of the medium-sized graupel (3-mm diameter) are presented to illustrate the process of differential motion within the echo.

The particles were released at 0.8 km at 1548 and followed backward in time to locate their source regions. The estimated fall speed of this low-density graupel (3 mm) is 2.5 m s^{-1} (from Pruppacher and Klett 1978) without adjusting for the air-density variation in the vertical. Figure 7 illustrates several representative graupel trajectories that arrive at 0.8 km and 1548. It is evident that there are two groups of particle trajectories as revealed in the air-trajectory computation, as discussed in Part I (Fig. 15 and 16 in Part I). The first group basically followed the up–down air trajectory but originated at 5 km, which is higher than the origin of the air parcels. These particles moved mainly in the meridional direction with a relatively small zonal component. The second group of particles mainly originated from the east to southeast of the storm and they moved around the up–down particles. The zonal trajectories exhibit westward transport near the north and south extrema of the echo. As a result, there was relative zonal motion between the center of the echo, composed of the up–down trajectories, and the north and south ends of the echo, composed of the zonal trajectories. Based on these trajectories, an elongated echo evolves into a bow shape by differential movement of hydrometeors between the center and the ends of the echo as a result of the initiation of the vorticity couplet.

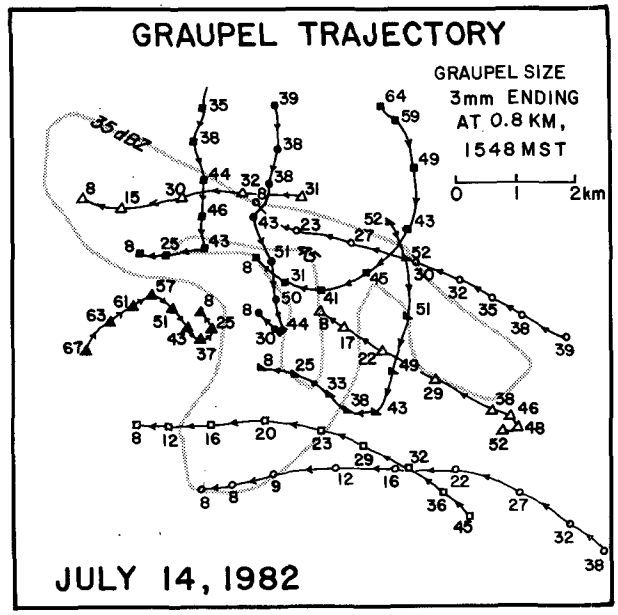

FIG. 7. The horizontal projection of the 3-mm graupel trajectories. The trajectory analysis is performed backward in time. The graupel is released at 0.8 km and 1548. The numbers are the height of graupel in 100 m. Reflectivity contours are 35, 40, and 45 dBZ_e. The time interval between symbols is 3 min.

In the next subsection, a vorticity-budget analysis is performed to address the origin of the vorticity couplet.

c. *Vorticity-budget analysis*

The change of vorticity with time can be evaluated by computing the vorticity equation. The vertical component of the relative vorticity ζ is defined as:

$$\zeta = \frac{\partial v}{\partial x} - \frac{\partial u}{\partial y}. \tag{1}$$

The vertical component of the vorticity equation derived from the anelastic (Ogura and Phillips 1962) horizontal momentum equations [Eqs. (1) and (2) in the Appendix of Part I] has the following form:

$$\frac{\partial \zeta}{\partial t} = \underbrace{-u\frac{\partial(\zeta+f)}{\partial x} - v\frac{\partial(\zeta+f)}{\partial y} - w\frac{\partial \zeta}{\partial z}}_{\text{advection terms}} - \underbrace{(\zeta+f)\nabla\cdot\mathbf{V}}_{\text{divergence term}} + \underbrace{\left(\frac{\partial w}{\partial x}\frac{\partial u}{\partial z} - \frac{\partial w}{\partial y}\frac{\partial u}{\partial z}\right)}_{\text{twisting or tilting term}}, \tag{2}$$

where f is the Coriolis parameter. All terms in (2) can be computed from the reconstructed multi-Doppler wind fields. There is no solenoidal term due to the use of the anelastic assumption and a constant mean virtual potential temperature. This technique has been used in past studies (Heymsfield 1981; Kessinger et al. 1988) to diagnose the source of thunderstorm rotation.

In this study, the multiple volumes of the wind fields permit the computation on both sides of (2). The vorticity equation is evaluated using a trapezoidal scheme. There are two independently computed vorticity tendencies, namely, the observed vorticity change between two successive volumes and the estimated vorticity tendency from the vorticity equation. It is believed that this approach is unique to allow for a cross-check between these two independent vorticity tendencies in this problem. If these two estimates agree with each other, then the origin and the evolution of the vorticity couplet can be identified from the forcing terms in the vorticity equation with confidence.

Figure 8 illustrates an example of the vorticity-budget computations at 2.4 km and 1546 where panel (a) is the observed vorticity tendency between the 1546 and 1548 volumes, panel (b) is the vorticity tendency predicted from the vorticity equation, and panels (c), (d), (e), and (f) are horizontal advection, vertical advection, divergence term, and tilting term, respectively. Terms in panels (c)–(f) are computed using the mean velocities between 1546 and 1548 (trapezoidal scheme). As a result, panel (b) represents the mean tendency between 1546 and 1548. Except for slight phase and amplitude differences, the vorticity equation [panel (b)] successfully predicts the observed vorticity tendency [panel (a)]. This agreement reveals the reliability of the reconstructed multi-Doppler wind fields.

The dipole structure of the vorticity tendency exists only in the tilting term due to the tilt of the horizontal vorticity into the vertical by the horizontal gradient of the downdraft. The magnitude of the vorticity tendency from the tilting term is nearly symmetric with a slightly stronger anticyclonic vorticity tendency. The cyclonic- (anticyclonic-) vorticity centers are located north (south) of the downdraft, respectively (downdraft stronger than -6 m s^{-1} is shaded). As predicted by a linear theory, this north–south vorticity couplet is produced by an eastward-pointing vertical shear vector (Rotunno and Klemp 1982). This agrees with the general environmental shear vector as shown in the Denver sounding (Fig. 3 in Part I). One must be cautious, however, in interpreting the eastward-pointing shear vector as the environmental shear vector since the thunderstorm circulation may have modified the environmental wind. The circulation associated with the vorticity couplet and perturbation pressure pattern (not shown) is similar to the "wake-entrainment" circulation reported in Knupp and Cotton (1985). The vorticity couplet in this study, however, is associated with a downdraft, not an updraft, as reported by Rotunno and Klemp (1982) and Knupp and Cotton (1985). Kingsmill and Wakimoto (1991) reported that the wake-entrainment mechanism is responsible for the initiation of a midlevel downdraft at approximately 9 km within an Alabama thunderstorm. Their finding is different from that presented in this study where the wake entrainment is a result of interaction between an existing downdraft and vertical shear.

The stronger positive vorticity tendency in Fig. 8b is contributed mainly from the downward advection of positive vorticity (Fig. 8d). The vorticity-budget computation at an earlier time indicates that this midlevel positive vorticity is also generated by the tilting of horizontal vorticity into the vertical by the updraft as suggested in Rotunno and Klemp (1982). Figure 9 shows an example of the vorticity generation by tilting term at 1536 at 4.8 km. The sign of the vorticity dipole is opposite to that produced by the downdraft with negative (positive) vorticity to the north (south). Recall that in Part I the updraft is tilted southward as it ascends. It follows that the precipitation forms over the positive vorticity. This positive vorticity is advected downward by the drag-induced downdraft at a later time.

The divergence term (Fig. 8e) also enhances the positive vorticity within the downdraft region by stretching the existing positive vorticity. The negative-vorticity region is not collocated with the intense downdraft region; therefore, the stretching effect is minimal in this region. Plots at lower levels (not shown), however, show that the divergence in the microburst outflow region (i.e., compression in the vertical) reduces the magnitude of the vorticity.

4. The conceptual model of the CBE

Based on the vorticity-budget analysis, we constructed a conceptual model of the evolution of this CBE event. The tilting of vortex tubes by updrafts and downdrafts in a convective storm has been illustrated in Klemp (1987). We adapt his concept and summarize the sequence of vorticity evolution of this CBE event in Fig. 10.

1) A convective cloud forms in an undisturbed environment with an eastward, unidirectional shear.

2) The horizontal vortex tube is tilted upward by the updraft, forming a vorticity couplet with positive and negative vorticity at the southern and northern side of the updraft, respectively.

3) As the downdraft initiates by falling precipitation, a new vorticity couplet with an opposite sign forms due to the interaction between the downdraft and the subcloud vertical shear of the horizontal wind. This downdraft also advects the positive vorticity downward. The combined effects of tilting, stretching, and downward advection produce stronger positive vorticity to the north and weaker negative vorticity to the south.

4) The differential motion of the hydrometeors due

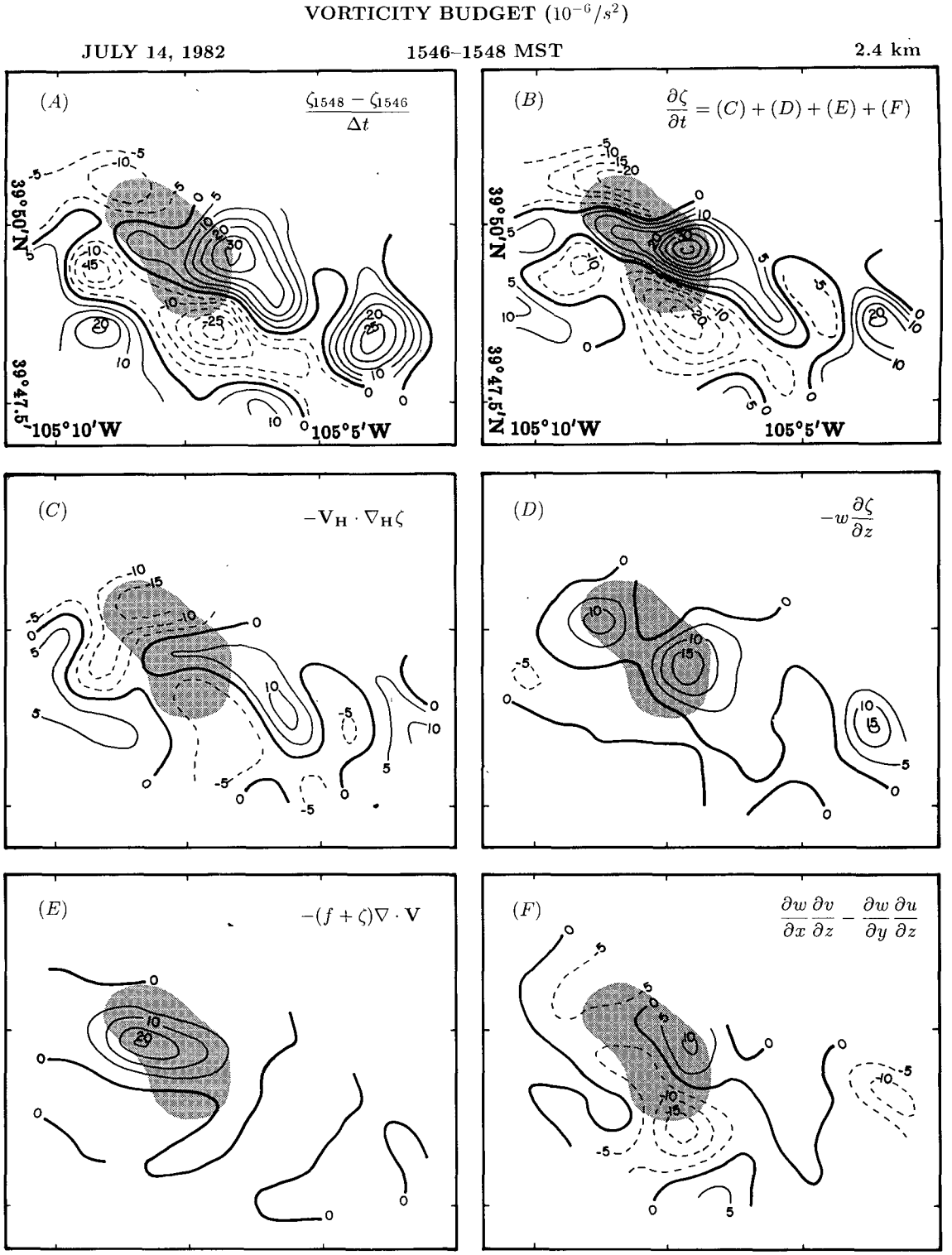

FIG. 8. The vorticity-budget computation from the reconstructed three-dimensional wind fields at 2.4 km of 1546 where (a) is the observed vorticity tendency between the 1546 and 1548 volumes, (b) is the vorticity tendency predicted from the vorticity equation for the same time period in (a), panels (c), (d), (e), and (f) are source terms in the vorticity equation: horizontal advection, vertical advection, divergence term, and tilting term, respectively. The unit is 10^{-6} s^{-2} and the downdraft greater than -6 m s^{-1} is shaded.

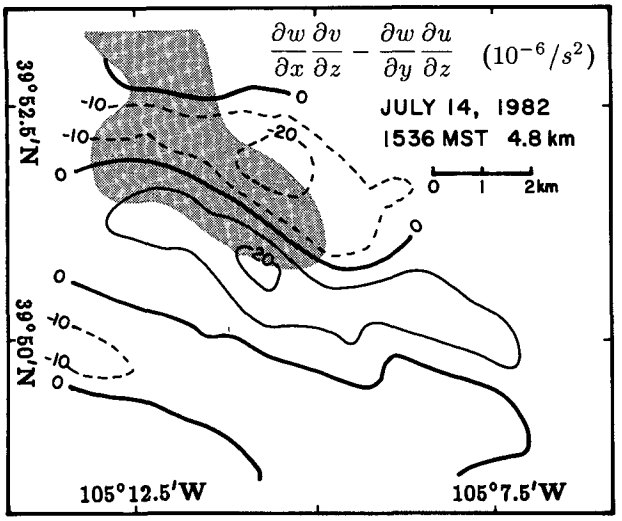

FIG. 9. The vorticity production by the tilting term at 4.8 km and 1536. The unit is 10^{-6} s^{-2} and the updraft greater than 6 m s^{-1} is shaded.

to the vorticity-couplet circulation distorts the elongated echo into a bow shape.

The existence of the vorticity couplet is the key factor in forming this bow echo. The generation of the vorticity couplet results from the product of the horizontal gradient of the downdraft and the vertical shear as given by the tilting term in (2). A vorticity couplet can be produced either by a strong downdraft in ordinary shear or by a weak downdraft with a stronger vertical shear. Once the vorticity is generated, Rotunno (1981) has shown that the stretching term can intensify the existing vorticity exponentially. Thus, the initial vorticity has a better potential to be stretched and to distort the echo by a strong downdraft than a weak downdraft. This is true especially in an airmass thunderstorm environment where the shear is often weak. This may be the reason why a CBE is often associated with strong wind events.

The effect of vertical advection depends on the updraft and downdraft structure. In this case, it results in an asymmetric vorticity pattern by enhancing either the positive or negative vorticity depending on the direction of the shear vector and the tilt of the updraft. If the updraft had tilted northward instead of southward, one might expect to have observed stronger negative vorticity. Another important factor is the unidirectional shear vector in the subcloud layer. If the subcloud shear vector is not unidirectional, the vorticity couplets at each level will not stack up vertically as they do in this case. Therefore, the hydrometeors might not be redistributed into a bow shape because of a complicated particle sedimentation–horizontal airspeed relationship.

One feature in this conceptual model of the CBE evolution that has not been discussed is the rear-inflow jet. As previously noted, this jet was observed consistently in previous SLBE and CBE cases. Based on the vorticity couplet circulation, flow between these two vortices would be enhanced to form a jetlike phenomenon. In a thunderstorm, the rear-inflow jet may be induced by the downdraft from mass continuity, or the vorticity-couplet circulation, or both. An inflow purely induced by mass continuity of the downdraft should not have directional preference. Therefore, the vorticity couplet must play an important role in determining the direction of the inflow from the rear of the storm.

In the 14 July bow-echo event, the rear-inflow jet exists in the ground-relative coordinates but does not exist in the storm-relative coordinates. This can be illustrated by superimposing a vorticity couplet with a westerly jet (as illustrated in Fig. 3) onto a uniform easterly mean flow with similar magnitude as the westerly jet. The resulting flow pattern should be similar to that presented in Fig. 6, having no westerly jet but rather strong easterlies outside both vorticity centers. This example demonstrates that a bow-shaped echo can form without a rear-inflow jet (storm-relative sense), thereby excluding the mechanism of echo erosion due to dry-air intrusion. With a similar mean flow, however, other bow echoes can have storm-relative rear-inflow jets if the magnitude of the jet is stronger than the mean flow by increasing the downdraft and/or the vertical shear. Under these circumstances, the dry air transported by the rear-inflow jet can promote the erosion of the echo by means of subsidence and evaporation/sublimation.

5. Photogrammetric analysis

A series of cloud photographs of the 14 July 1982 bow-echo–microburst storm were taken at the CP-3 radar site between 1548 and 1554. By applying photogrammetric techniques (Holle 1988), the azimuth and elevation angle on the cloud photograph relative to the CP-3 radar can be determined. Then, the CP-3 radar reflectivity factor and projection of the reconstructed three-dimensional velocities on any particular plane can be superimposed onto the cloud photo (Lee 1989; Kingsmill and Wakimoto 1991). Figure 11a illustrates the visual appearance of this bow-echo–microburst event at 1549 superimposed with the CP-3 radar reflectivity factor from the 1548–1550 volume. The projection of the three-dimensional velocities through the microburst center within the bow echo is superimposed on the cloud photo (Fig. 11b). The perspective view, labels, and locations of the superimposed reflectivity values (indicated by circles) of the bow echo are shown in Fig. 11c. The CP-3 reflectivity values are chosen as the maximum values in a specific azimuth and elevation angle except in the southern part of the storm where the bow echo is masked by an appendage echo. The center of the microburst (the maximum dif-

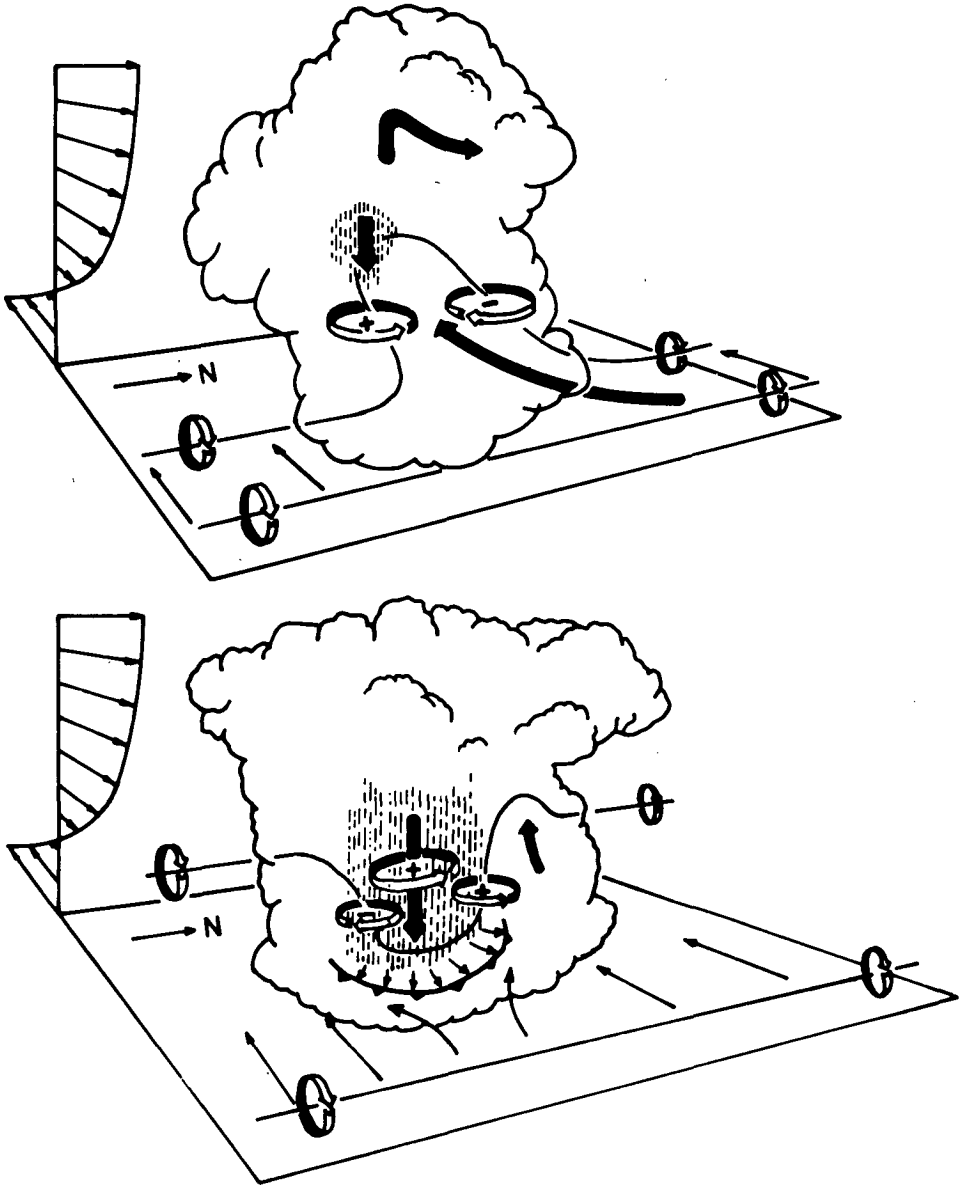

FIG. 10. The conceptual model of the vorticity evolution within a CBE (adapted from Klemp 1987).

ferential velocity) determined from the display of the radial Doppler velocities is along the 256° azimuth from the CP-3 radar. The microburst center is located at the weak-echo notch in between two 50-dBZ_e reflectivity maxima. It coincides with the visually light rain area (transparent area marked as the precipitation hole) where the maximum downdraft occurs as shown by the multi-Doppler winds in Fig. 11c. The darkest rain shaft between 240° and 250° is associated with a reflectivity factor of 30–40 dBZ_e.

Key features noted in this analysis are

1) A visually heavy (dark) rain shaft is not necessarily associated with a high-reflectivity region and strong downdrafts, a result that is also found within a dry microburst (Wakimoto 1988).

2) The precipitation hole (light rain-shaft area) that is safe visually to a pilot may be the most dangerous place for aircraft penetration.

6. Discussion

a. Bow echo and echo notch

There is no clear-cut distinction in the echo shape between an echo "notch" and a bow echo. Based on the reflectivity pattern, a bow echo has a notch but not every echo notch can be classified as a bow echo. We

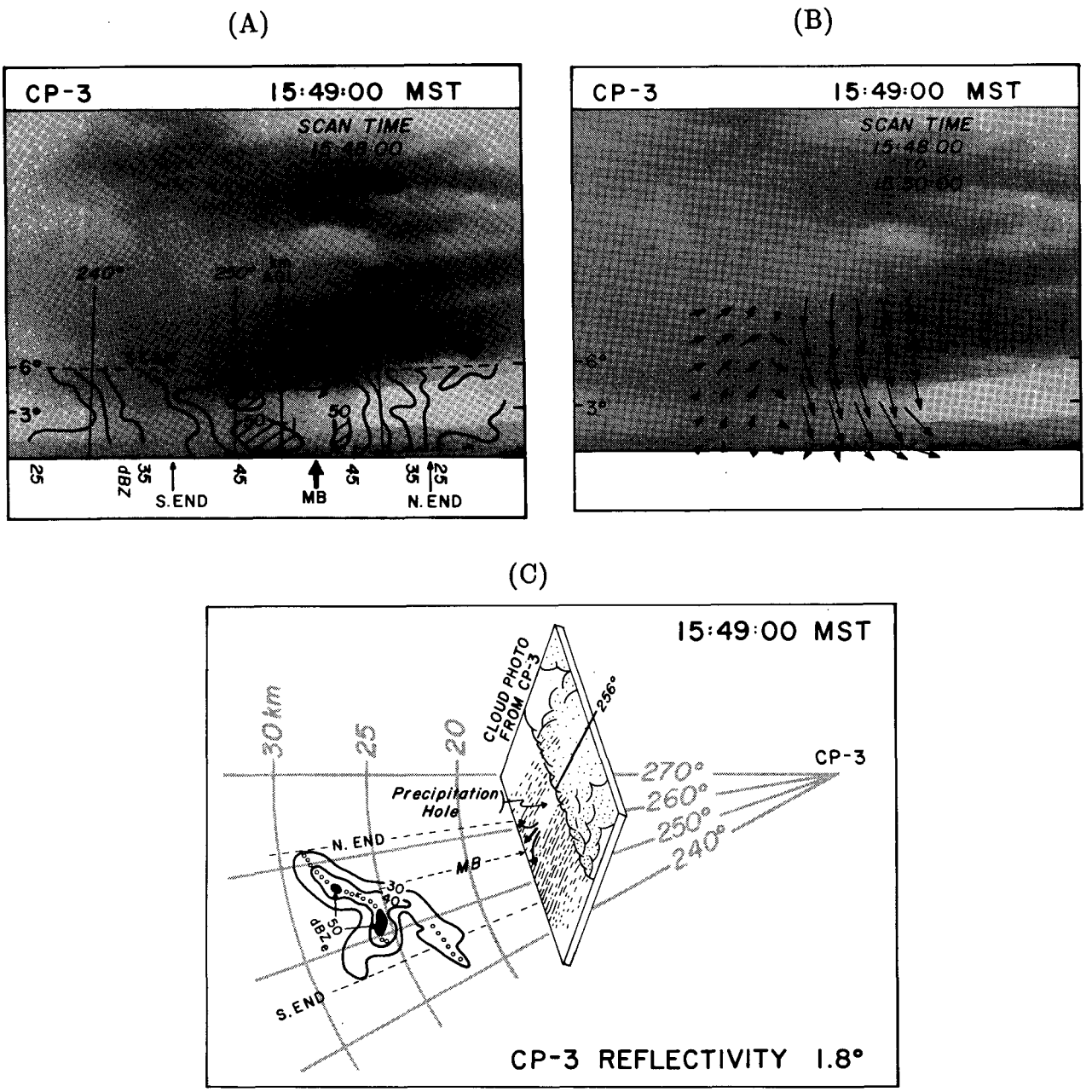

FIG. 11. (a) Cloud photo of the 14 July 1982 bow-echo–microburst storm at 1549 from the CP-3 Doppler radar site. The maximum reflectivity factor at each azimuth and elevation angle was superimposed on the photo via a photogrammetry technique. A region that is visually transparent is marked "precipitation hole." (b) The projection of the 3D wind fields through the microburst center along the bow echo onto the cloud photo. (c) Perspective view of the cloud photo in (a). The circles within the bow echo are the locations where the reflectivity factors are chosen.

have demonstrated that certain environmental conditions and dynamical processes such as unidirectional environmental shear and the tilting of horizontal vorticity by the downdraft into the vertical are related to the evolution of bow echoes. The distortion of an elongated echo into a bow shape indicates the occurrence of a possible microburst and can be identified by a ground-relative rear-inflow jet on the Doppler velocity display if the radar is not scanning perpendicular to the direction of storm motion. Conversely, notches can be produced not only by the preceding mechanism but also by inflow of environmental dry air (Elmore 1986; Knupp 1989; Robert and Wilson 1989), by irregular-shaped or multiple updrafts (such as the appendage in

this case) or by merging of two thunderstorms that may not be associated with bow-echo processes. Echo notches produced by other mechanisms are observed commonly within convective storms. In order to capture the bowing process and the development of a rear-inflow jet of a CBE, a Doppler radar must scan at higher elevation angles and we must combine both the reflectivity and Doppler velocity information in identifying the bow echo.

b. *Similarity between the CBE and SLBE*

Weisman (1990) simulated long-lived, steady SLBEs using a three-dimensional cloud model. He identified favorable environmental conditions, such as unidirectional vertical shear (at least 20 m s^{-1} over the lowest 2.5 km) and a convective available potential energy (at least 2000 m^2 s^{-2}), in forming SLBEs. The bow echo forms after several hours of simulation and is characterized by "bookend" vortices and a rear-inflow jet. The rear-inflow jet and the bow-echo structure always develop after the occurrence of the bookend vortices. These vortices, which are produced by tilting the horizontal vorticity into vertical, are essentially the same phenomenon as the vorticity couplet resolved in this study. The intensity of the rear-inflow jet is partly contributed from the bookend vortices (~40%–50%) and the horizontal vorticity generation by the baroclinic term (the cold pool at the surface and the latent heat release at high levels).

The similarity between the simulated SLBE above and the CBE in this study resides in the tilting of vorticity by the downdraft that exists in both the observation (the vorticity couplet) and model simulation (bookend vortices). Apparently, the primary difference between the SLBE and the CBE is in the baroclinically generated horizontal vorticity. The baroclinic effect (vertical temperature difference) also exists in this CBE; however, the time scale in a short-lived airmass thunderstorm is not long enough to generate significant horizontal vorticity. This is probably why the rear-inflow jet observed in SLBEs is stronger than that in the CBEs in the cases mentioned in this paper. Another factor, the Coriolis effect, is also more important to the SLBEs than the CBEs due to the spatial-scale differences. In the Northern Hemisphere, the Coriolis effect would promote the cyclonic rotation of the storm or the line that agrees with the conceptual model proposed by Fujita (1981).

7. Summary and conclusions

Using a vorticity-budget study based on the reconstructed 3D wind field of the 14 July 1982 bow-echo–microburst event, we have evaluated the evolution of a CBE and the bow-echo–microburst relationship. This is believed to be the first complete quantitative study of the evolution of a CBE.

In contrast to SLBEs, this CBE does not exhibit a rear-inflow jet in the storm-relative coordinates. This bow echo evolves from an elongated echo by redistributing hydrometeors from the center to both ends of the echo due to the vorticity couplet circulation. This vorticity couplet is associated with a stronger cyclonic vorticity to the north (maximum of 6×10^{-3} s^{-1}) and weaker anticyclonic vorticity (maximum of -4×10^{-3} s^{-1}) to the south of the downdraft that did not exist before the initiation of the downdraft. The couplet first forms below the cloud base and subsequently propagates downward as the downdraft evolves. The bow echo at the surface reflects the shape of the echo aloft as hydrometeors descend. The location of the microburst coincides with the weak-echo notch of the bow echo at the surface. The vorticity-budget study indicates that this vorticity couplet is produced by the horizontal gradient of w across the downdraft, which tilts the horizontal vorticity into vertical. The microburst outflow below 0.8 km deflects the environmental flow and enhances the echo distortion.

Major findings in this study are 1) An elongated echo can evolve into a CBE if (a) there is an unidirectional vertical shear and (b) a downdraft exists. 2) An elongated echo may be distorted into a bow echo through the redistribution of hydrometeors by a vorticity couplet. The intensity of the vorticity couplet is determined by the product of the vertical shear and horizontal gradient of the downdraft. This vorticity couplet subsequently may be intensified by the stretching of the downdraft. 3) A storm-relative rear-inflow jet is not essential to the formation of a CBE. 4) A CBE is neither a sufficient nor a necessary condition for the existence of a strong downdraft. It only *indicates* the existence and the location of a downdraft. Due to generally weak vertical shear in the airmass thunderstorm environment, however, the distortion of an echo into a bow shape often requires a strong downdraft. This, combined with a rear-inflow jet in the Doppler radial velocity field, can be a useful radar signature for both the NWS and air-traffic controllers in nowcasting the general likelihood of strong downdrafts and damaging wind events. 5) Photogrammetric analysis of this event suggested that the intensity of the downdraft may not be correlated with the darkness of the rain shaft. This is important information for pilots to understand for general guidance in storm penetration.

Acknowledgments. A Graduate Research Assistantship awarded by the Advanced Study Program at NCAR to the first author is greatly appreciated. The first author is enormously grateful to his Ph.D. committee members A. Arakawa, C. Friehe, R. Kelly, and M. Yanai for many simulating discussions and helpful comments. The first author is very grateful to the scientists and staff of the Atmospheric Technology Division and Mesoscale and Microscale Meteorology Di-

vision during his residence at NCAR. We would like to thank J. Wilson, C. Mueller, C. Kessinger, M. Hjelmfelt, R. Roberts, K. Elmore, R. Oye, J. Corbet, and C. Burghart for their assistance and valuable discussions in Doppler radar data processing, RDSS and the ODDAN software. We would also like to thank J. Miller, C. Mohr, D. Parsons, and J. Tuttle for their kind assistance in the CEDRIC software, thermodynamic retrieval, and the trajectory analysis. The cloud photos were taken by Brian Smith of the University of Chicago. We acknowledge D. Kingsmill of UCLA for his help in preparing figures and valuable discussions throughout this research. C. Kippes and T. Weckwerth are acknowledged for proofreading this manuscript. We are grateful to anonymous reviewers whose comments led to improvements and clarity of this manuscript. This research was supported by the National Science Foundation under Grants NSF ATM 83-19486, ATM 87-03143, and ATM 90-08683.

REFERENCES

Elmore, K. L., 1986: Evolution of a microburst and bow-shaped echo during JAWS. Preprints, *23d Conf. on Radar Meteorology,* Snowmass, Amer. Meteor. Soc., J101–J104.

Forbes, G. S., and R. M. Wakimoto, 1983: A concentrated outbreak of tornadoes, downbursts and microbursts, and implications regarding vortex classification. *Mon. Wea. Rev.,* **111,** 220–235.

Fujita, T. T., 1978: Manual of downburst identification for project NIMROD. Satellite and Mesometeorology Research Paper No. 156, Dept. of Geophysical Sciences, Univ. of Chicago, 104 pp. [NTIS PB-286048.]

——, 1981: Tornadoes and downbursts in the context of generalized planetary scales. *J. Atmos. Sci.,* **58,** 1164–1181.

——, 1985: *The Downburst: Microburst and Macroburst.* The University of Chicago Press, 122pp. [NTIS PB 86-131638.]

——, and H. R. Byers, 1977: Spearhead echo and downburst in the crash of an airliner. *Mon. Wea. Rev.,* **105,** 129–146.

——, and F. Caracena, 1977: An analysis of three weather-related aircraft accidents. *Bull. Amer. Meteor. Soc.,* **58,** 1164–1181.

Hamilton, R. E., 1970: Use of intensity radar data in mesoscale surface analysis of the July 4, 1969 storm in Ohio. Preprints, *14th Conf. on Radar Meteorology,* Edmonton, Amer. Meteor. Soc., 339–346.

Heymsfield, G. M., 1981: Evolution of downdrafts and rotation in an Illinois thunderstorm. *Mon. Wea. Rev.,* **109,** 1969–1988.

Hinrichs, G., 1888: Tornadoes and derechos. *Amer. Meteor. J.,* **5,** 306–317.

Holle, R. L., 1988: Photogrammetry of thunderstorms. *Instruments and Techniques for Thunderstorm Observation and Analysis,* E. Kessler, Ed., University of Oklahoma Press, Norman, 51–64.

Johns, R. H., and W. D. Hirt, 1983: The derecho—A severe weather producing convective system. Preprints, *13th Conf. Severe Local Storms,* Amer. Meteor. Soc., 178–181.

Kessinger, C. J., D. B. Parsons, and J. W. Wilson, 1988: Observations of a storm containing misocyclones, downbursts, and horizontal vortex circulations. *Mon. Wea. Rev.,* **116,** 1959–1982.

Kingsmill, D. E., and R. M. Wakimoto, 1991: Kinematic, dynamic and thermodynamic analysis of a weakly sheared severe thunderstorm over northern Alabama. *Mon. Wea. Rev.,* **119,** 262–297.

Klemp, J. B., 1987: Dynamics of tornadic thunderstorms. *Ann. Rev. Fluid Mech.,* **19,** 369–402.

Knupp, K. R., 1989: Numerical simulation of low-level downdraft initiation within precipitation cumulonimbi: Some preliminary results. *Mon. Wea. Rev.,* **117,** 1517–1529.

——, and W. R. Cotton, 1985: Convective cloud downdraft structure: An interpretive survey. *Rev. Geophys.,* **23,** 183–215.

——, and D. P. Jorgensen, 1985: Case study analysis of a large-scale and long-lived downburst-producing storm. Preprints, *14th Conf. on Severe Local Storms,* Indianapolis, Amer. Meteor. Soc., 301–304.

Lee, W.-C., 1989: The evolution and structure of the bow echo/microburst events. Cooperative Thesis No. 117, University of California at Los Angeles and National Center for Atmospheric Research, 261pp. [University Microfilms International #8906408.]

——, R. E. Carbone, and R. M. Wakimoto, 1992: The evolution and structure of a "bow-echo–microburst" event. Part I: The microburst. *Mon. Wea. Rev.,* **120,** 2188–2210.

McCarthy, J., J. W. Wilson, and T. T. Fujita, 1982: The Joint Airport Weather Studies Project. *Bull. Amer. Meteor. Soc.,* **63,** 15–22.

Miller, L. J., J. D. Tuttle, and C. A. Knight, 1988: Airflow and hail growth in a severe northern High Plains supercell. *J. Atmos. Sci.,* **45,** 736–762.

Nolen, R. H., 1959: A radar pattern associated with tornadoes. *Bull. Amer. Meteor. Soc.,* **40,** 277–279.

Ogura, Y., and N. A. Phillips, 1962: Scale analysis of deep and shallow convection in the atmosphere. *J. Atmos. Sci.,* **19,** 173–179.

Pruppacher, H. R., and J. D. Klett, 1978: *Microphysics of Clouds and Precipitation.* D. Reidel, 715pp.

Przybylinski, R. W., and W. J. Gery, 1983: The reliability of the bow echo as an important severe weather signature. Preprints, *13th Conf. on Severe Local Storms,* Tulsa, Amer. Meteor. Soc., 270–273.

——, and D. M. DeCaire, 1985: Radar signatures associated with the derecho, a type of mesoscale convective system. Preprints, *14th Conf. on Severe Local Storms,* Indianapolis, Amer. Meteor. Soc., 228–231.

Roberts, R. D., and J. W. Wilson, 1989: A proposed microburst nowcasting procedure using Doppler radar. *J. Appl. Meteor.,* 285–303.

Rotunno, R., 1981: On the evolution of thunderstorm rotation. *Mon. Wea. Rev.,* **109,** 577–586.

——, and J. B. Klemp, 1982: The influence of shear induced pressure gradient on thunderstorm motion. *Mon. Wea. Rev.,* **110,** 136–151.

Schmidt, J. M., and W. R. Cotton, 1989: A High Plains squall line associated with severe surface winds. *J. Atmos. Sci.,* **46,** 281–302.

Smull, B. F., and R. A. Houze, 1985: A mid-latitude squall line with a trailing region of stratiform rain: Radar and satellite observations. *Mon. Wea. Rev.,* **113,** 117–133.

Stout, G. E., and F. A. Huff, 1953: Radar records Illinois tornadogenesis. *Bull. Amer. Meteor. Soc.,* **34,** 281–284.

Wakimoto, R. M., 1983: The West Bend, Wisconsin storm of 4 April 1981: A problem in operational meteorology. *J. Climate Appl. Meteor.,* **22,** 181–189.

——, 1988: Operational aspects of a microburst-producing storm during MIST. Preprints, *15th Conf. on Severe Local Storms,* Baltimore, Amer. Meteor. Soc., 384–387.

Weisman, M. L., 1990: The genesis of bow echoes: A rear-inflow induced meso-convective structure. Cooperative Thesis No. 125, The Pennsylvania State University and National Center for Atmospheric Research. 149pp.

Wright, J. E., 1985: Observation of bow echoes with the Marseilles radar system. Preprints, *14th Conf. on Severe Local Storms,* Indianapolis, Amer. Meteor. Soc., 309–312.